Lab on a Chip

Accepted Manuscript

This is an *Accepted Manuscript*, which has been through the Royal Society of Chemistry peer review process and has been accepted for publication.

Accepted Manuscripts are published online shortly after acceptance, before technical editing, formatting and proof reading. Using this free service, authors can make their results available to the community, in citable form, before we publish the edited article. We will replace this *Accepted Manuscript* with the edited and formatted *Advance Article* as soon as it is available.

You can find more information about *Accepted Manuscripts* in the **Information for Authors**.

Please note that technical editing may introduce minor changes to the text and/or graphics, which may alter content. The journal's standard **Terms & Conditions** and the **Ethical guidelines** still apply. In no event shall the Royal Society of Chemistry be held responsible for any errors or omissions in this *Accepted Manuscript* or any consequences arising from the use of any information it contains.

TOC Graphical Abstract

Capture and enumeration of mRNA transcripts from single cells using a microfluidic device†

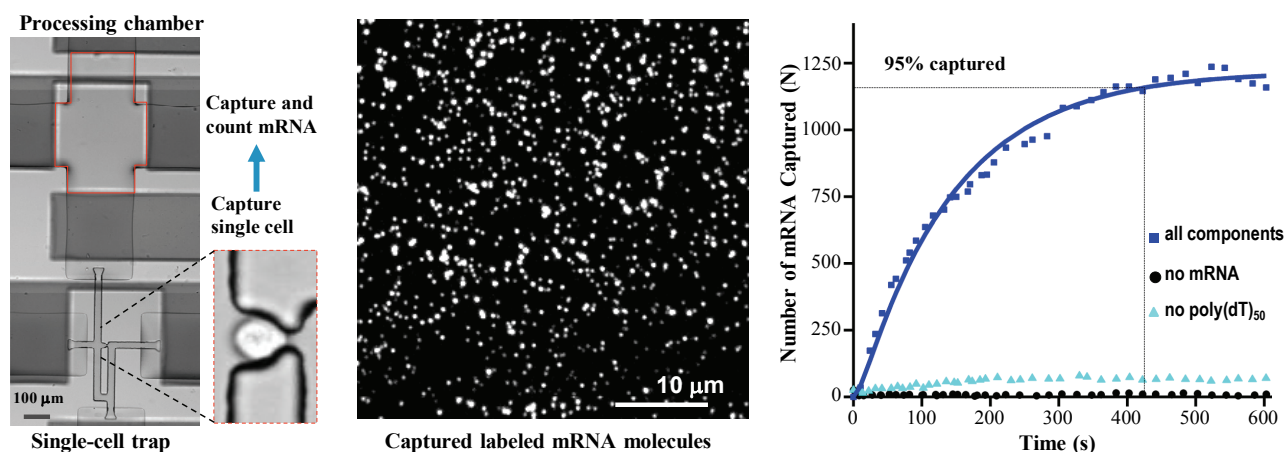Matthew T. Walsh,[a§] Alexander P. Hsiao,[a§] Ho Suk Lee,[b] Zhixia Liu,[a] and Xiaohua Huang[a*]

[a]Department of Bioengineering, University of California, San Diego, La Jolla, CA 92093-0412, USA.
[b]Department of Electrical and Computer Engineering, University of California, San Diego, La Jolla, CA 92093.
[§]These authors contributed equally to this work.
*Address correspondence to Prof. Xiaohua Huang. Tel: +01-858-822-2155. E-mail: x2huang@ucsd.edu.

We report an integrated microfluidic device for direct capture and digital counting of polyadenylated mRNA molecules from single cells.

Processing chamber

Capture and count mRNA

Capture single cell

100 μm

Single-cell trap

Captured labeled mRNA molecules

10 μm

95% captured

Number of mRNA Captured (N)

all components
no mRNA
no poly(dT)$_{50}$

Time (s)

Lab on a Chip

ROYAL SOCIETY OF CHEMISTRY

Capture and Enumeration of mRNA Transcripts from Single Cells Using a Microfluidic Device†

Matthew T. Walsh,[a][§] Alexander P. Hsiao,[a][§] Ho Suk Lee,[b] Zhixia Liu,[a] and Xiaohua Huang[a]*

Accurate measurement of RNA transcripts from single cells will enable the precise classification of cell types and characterization of the heterogeneity in cell populations that play key roles in normal cellular physiology and diseases. As a step towards this end, we have developed a microfluidic device and methods for automatic hydrodynamic capture of single mammalian cells and subsequent immobilization and digital counting of polyadenylated mRNA molecules released from the individual cells. Using single-molecule fluorescence imaging, we have demonstrated that polyadenylated mRNA molecules from single HeLa cells can be captured within minutes by hybridization to polydeoxyribothymidine oligonucleotides covalently attached on the glass surface in the device. The total mRNA molecule counts in the individual HeLa cells are found to vary significantly from one another. Our technology opens up the possibility of direct digital enumeration of RNA transcripts from single cells with single-molecule sensitivity using a single integrated microfluidic device.

Introduction

A central focus of biology is to understand quantitatively how an organism's genotype determines its phenotype. The phenotypes of the different cell types in a multi-cellular organism are defined by the selective expression of the genome to produce a unique set of RNA molecules (the transcriptome) and protein molecules (the proteome) that carries out the characteristic physiological functions of the cells. Due to the technical difficultly in whole proteome analysis, the transcriptomes are often used as surrogates to assess the physiological states of cells. Gene expression varies greatly amongst individual cells, even within a population of the same cell type and the subtle differences may contribute significantly to normal cellular physiology such as stem cell differentiation and abnormal cellular physiology such as cancer.[1-5] The ability to precisely and quantitatively measure whole transcriptomes at the single-cell level is essential to measure cellular heterogeneity and to define cell types.

Methods have been developed for direct detection and counting of DNA and RNA molecules in single cells, usually by *in situ* hybridization and single-molecule fluorescence imaging.[6-11] However, only a limited number of RNA species can be analyzed using these methods. Comprehensive transcriptome profiling of single cells is now feasible using methods based on high throughput sequencing such as RNA-seq[12-15] or direct single-molecule RNA sequencing.[16-18] But a large amount of input materials, equivalent to tens to thousands of cells is required, necessitating the amplification of the transcripts for single-cell analysis. Amplification is known to introduce bias into the relative abundance of the transcripts, in particular the ones with lower copy numbers, compromising the accuracy of the measurements.[13, 19] The bias can be significantly mitigated by integrating the processes for cell isolation, RNA extraction, cDNA synthesis and amplification using microfluidic devices.[13] The small processing volumes in microfluidic devices help minimize sample loss and improve the efficiency of reactions by maintaining high concentrations of biomolecules[13, 20-22]. These devices can be used to perform RT-qPCR quantification of RNA transcripts, albeit on only a limited number of RNA species, from single cells[23-26], cell monitoring[27] and chip-based analysis.[28, 29] So far, the current generation of microfluidic devices still lacks the capability for comprehensive direct on-chip detection and digital counting of RNA transcripts from single cells.

We present a microfluidic platform that enables the capture, isolation, and lysis of single cells, and the on-chip capture and

[a]Department of Bioengineering, University of California, San Diego, La Jolla, CA 92093, USA.

[b]Department of Electrical and Computer Engineering, University of California, San Diego, La Jolla, CA 92093, USA

[§]These authors contributed equally to this work.

*Corresponding author. Email: x2huang@ucsd.edu

Lab on a Chip Accepted Manuscript

enumeration of the total polyadenylated mRNA molecules by single-molecule fluorescence imaging. Single cells are captured along a series of hydrodynamic traps and isolated by polydimethylsiloxane (PDMS) valves. The cells are then chemically lysed in individual compartments where polyadenylated (poly(A)) mRNA molecules are captured by hybridization onto polydeoxyribothymidine oligos (poly(dT)) functionalized on the glass surface. We also report a method for the selective functionalization of the PDMS and glass surfaces in the microfluidic devices, enabling the efficient capture of mRNA molecules from single cells and single-molecule fluorescence imaging. We use time-lapse single-molecule fluorescence imaging and numeric simulations to determine the kinetics of mRNA capture. It is shown that the mRNA molecules in the microfluidic chambers diffuse down and hybridize to the poly(dT) oligos on the surface very rapidly, to almost completion within minutes. As a proof of principle, we analyze the total number of polyadenylated mRNA molecules from individual HeLa cells.

Materials and Methods

Materials

Synthetic oligonucleotides (oligos) were purchased from Integrated DNA Technologies. A monofunctional amine-PEG with MW of ~2000 g/mol (amine-PEG2000) and a homo-bifunctional carboxymethyl polyethylene glycol with a molecular weight of 1000 g/mol (dicarboxyl-PEG1000) were purchased from Laysan Bio, Inc. Dulbecco's Modified Eagle's Medium (DMEM) were purchased from Mediatech, Inc. More information is provided in the ESI.

Microfluidic device design and operation

The design of our device is illustrated in Fig. 1. Our device consists of 16 modules for parallel processing of 16 cells (Fig.1a). Each module contains a hydrodynamic cell trap and a compartment for processing and imaging (Fig.1b). The single-cell hydrodynamic traps are adapted from the work of Tan *et al.*[30] and the principle of operation is illustrated in Fig.1c. Each trap chamber has two flow paths, one through a cell trap and one through a bypass. In this work, our trap path is designed as a small channel with 8 µm x 8 µm cross section with a round 22 µm x 22 µm cup-shaped mouth.
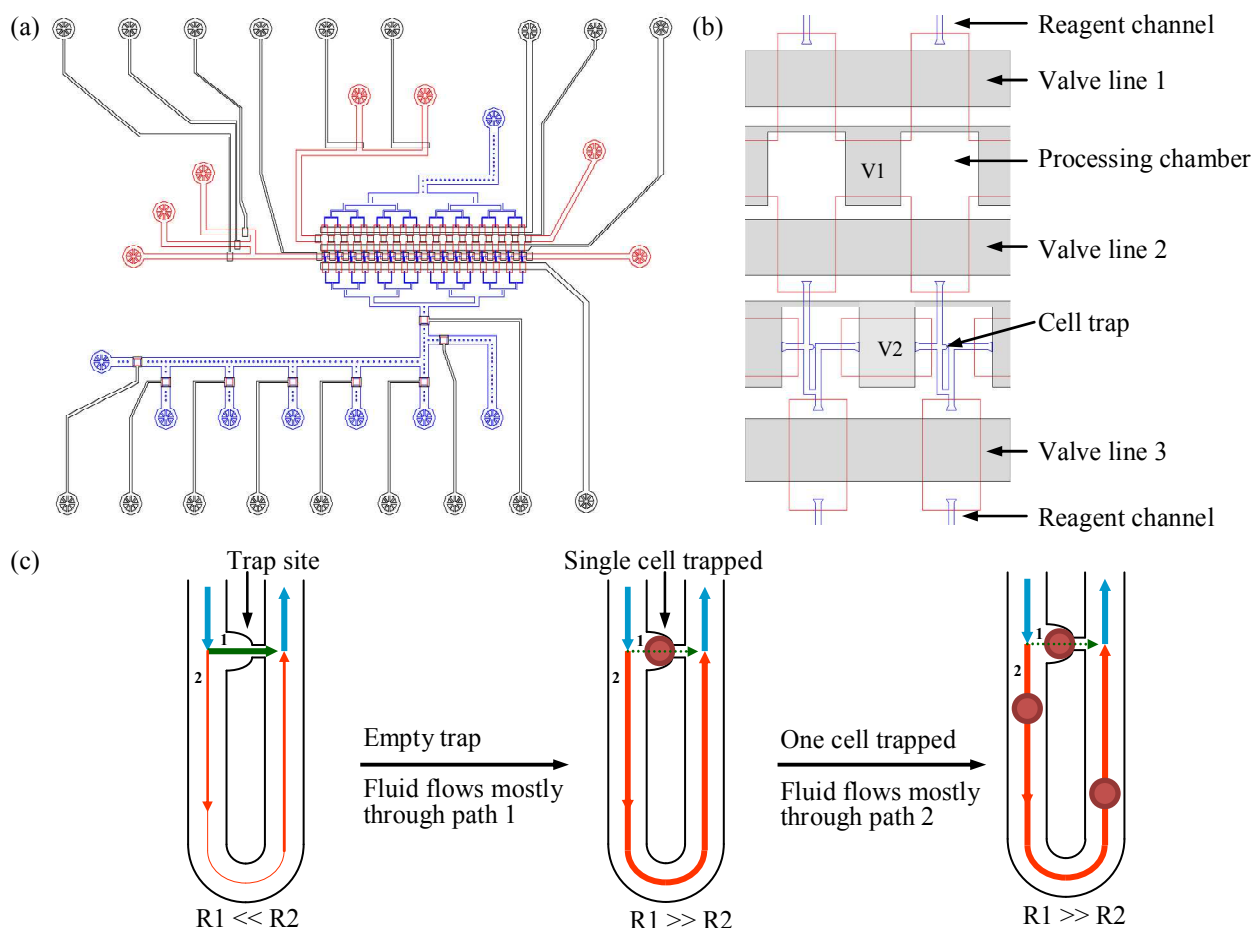

Fig. 1 Design and operation of the microfluidic device for capturing and counting of mRNA molecules from single cells. (a) 2D CAD layout of a device with 16 modules in serial. Red: fluid channels and chambers with 25 µm height; Blue: Fluidic channels/chambers with 25 µm height; Black: valves and valve control lines with 40 µm height. (b) An enlarged portion of the device containing two modules. The valves (V1 and V2) and valve lines are shown in light grey. Each module consists of a cell trap and a processing chamber. (c) Hydrodynamic trap design and operation. The in-flowing fluid is split into two paths, the cell trap (path 1) and bypass (path 2). The dimensions of the paths are designed such that the fluidic resistance through cell trap path (R1) is much smaller than that of the bypass (R2). In the empty trap, the fluid and cells preferentially flow into the trap path. The entry and trapping of the first single cell results in an abrupt increase in the fluidic resistance of path 1 and the fluid flow is then directed to the bypass (path 2) to the next trap in series, and so on.

The dimensions of the paths are designed such that the cell trap path has a much lower fluidic resistance than the bypass path. Therefore, the bulk of fluid containing the cells is channeled into the single-cell trap. Any incoming cell that is larger than the narrow cross-section of the trap will be captured. Upon trapping of the first cell, the path is immediately blocked and the fluid containing additional cells is diverted into the bypass to the next trap in series. Our design is guided by simulations using finite element analysis method to ensure high-efficiency capture of single cells. The microfluidic module in COMSOL Multiphysics (COMSOL Inc.) is used for the simulations. The flow is assumed to be laminar. The flow velocity at the inlet is set to a fixed value while the pressure at the outlet is set to zero and all boundaries are set to a no-slip condition.

Orthogonal to the direction of cell capture channel are the compartments for cell lysis, RNA capture and further processing (Fig.1b). The glass surface of this compartment is functionalized with 50-base poly(dT) oligos to capture the polyadenylated mRNA molecules by hybridization. The cell suspension is flowed into the trap channel after valve lines 2 and 3 are actuated to isolate the cell trap channel from the reagent channels and processing chambers. Upon successful single-cell trapping, the valves between the modules (V1 and V2) are then closed to compartmentalize the cells. The individual cells are then moved upward by injecting a lysis solution from the lower reagent channels into the processing chambers where the cells are lysed and the released poly(A) mRNA molecules are captured onto the glass surface by hybridization.

PDMS device fabrication

The PDMS devices were designed and fabricated according to the procedures of Unger et al.[31] with some modifications as described in our previous work.[32, 33] A two-step lithography process was utilized to fabricate the mold for the PDMS fluidic layer with larger rounded channels for valving and smaller channels with vertical walls for cell trapping and fluid flow. All fluidic channels were fabricated to a height of 25 μm. The width and length of the processing chamber are 250 μm. The mold for the valve control layer was patterned with a channel height of 40 μm.

The valve control layer and fluidic channel layer were prepared using Sylgard 184 (Dow Corning) with part A to part B ratio of 5:1 and 20:1, respectively. The valve control layer was prepared by adding degassed PDMS prepolymer mixture onto the mold in a carrier. The fluidic channel layer was prepared by spin-coating of degassed PDMS mixture onto the mold to a height of about 50 μm. After the PDMS layers were cured at 65 °C for 30 min., the valve control PDMS layer was peeled off the mold and holes were punched for fluidic connections using a 0.75 mm diameter punch. The two layers were bonded together by heating at 65 °C for 4 hours. The bonded PDMS layers were peeled off the mold together and holes were punched for the fluidic connections. The detailed procedures are provided in the ESI.

Chemical bonding of PDMS to glass and selective functionalization of surfaces

The overall process is illustrated in Fig. 2. First, the bottom of the PDMS channel layer is covalently bonded onto a glass coverslip by a chemical reaction between the reactive groups functionalized on their surfaces.[34] Briefly, the surface of the PDMS layer was activated by oxygen plasma in a UV-ozone cleaner and functionalized with epoxy groups using 3-glycidoxypropyl triethoxysilane while the surface of the cover glass is activated with primary amine groups using 3-aminopropyltriethoxysilane. Then the PDMS layer was laid onto and bonded to the coverslip by heating at 60 °C for 4 hours to crosslink the epoxy groups and the amine groups on their surfaces. Second, the surface of the PDMS inside the channels was passivated with polyethylene glycol (PEG) by reacting the epoxy groups with the amine groups on monofunctional amine-PEG2000. Third, the amine groups on the glass surface were converted to carboxyl groups by reacting with bifunctional bicarboxyl PEG1000 in large excess. Any residual unreacted amine was converted to acetyl amide using sulfosuccinimidyl acetate. Finally, the glass surface in the processing chambers was selectively functionalized with poly(dT)$_{50}$ oligos using 5'-amine-labeled poly(dT)$_{50}$ oligos. All channels were then washed with and stored in saline sodium citrate buffer until use. The detailed procedures are provided in the ESI.
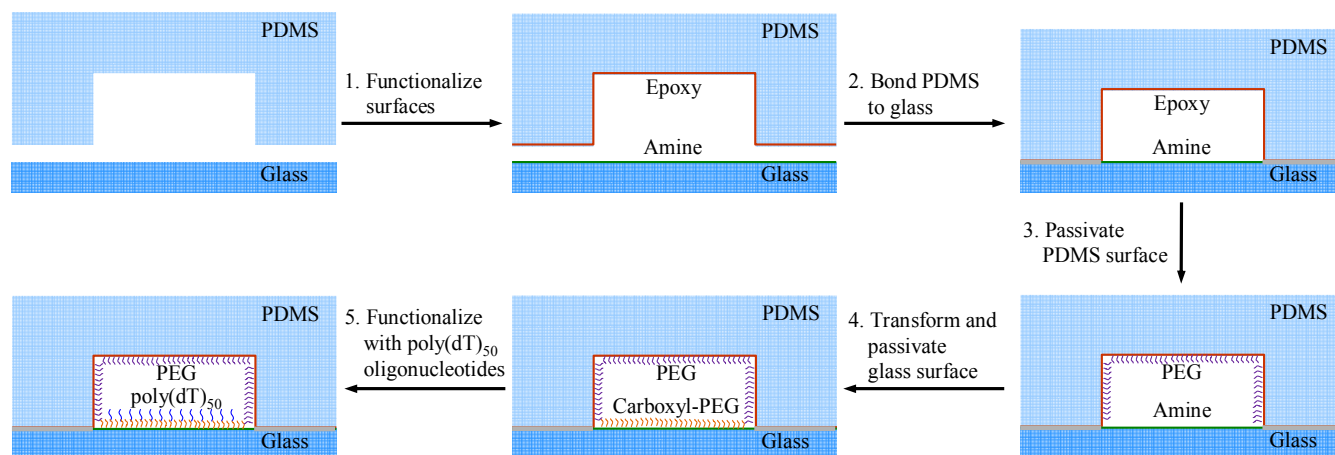

Fig. 2 Method for chemical bonding and selective functionalization of the surfaces of the microfluidic devices. The novel strategy allows for the chemical bonding of PDMS to a glass substrate and selective passivation of the PDMS surface and functionalization of the glass surface.

Preparation of fluorescently-labeled synthetic mRNA

The mRNA is transcribed from a gene encoding a phi29 DNA polymerase on a plasmid. A 30-cycle PCR was performed to amplify the gene with a primer to include the T7 promoter and a primer designed to include a 150-base poly(dT) tail. The PCR product was used as a template to transcribe the mRNA in the presence of fluorescein-12-UTP (Enzo Life Sciences) at 2% of the total UTP concentration using the HiScribe™ T7 transcription Kit (New England Biolabs). After digest of the DNA using DNase-I, the polyadenylated fluorescein-labeled mRNA was purified using a kit (MEGAclear Kit, Ambion) and murine RNase inhibitor (Roche) was added into the product to prevent degradation. The final mRNA product is about 1700 base long and contains a 150-base poly(A) tail (termed poly(A)$_{150}$-phi29 mRNA for short). The concentration of the product and average number of labels per molecule were quantified by UV-vis absorption.

Cell culture and preparation

HeLa cells were grown and maintained under standard culture conditions (37 °C and 5% CO$_2$) in DMEM supplemented with 10% fetal bovine serum and 1% penicillin/streptomycin. The cells were detached from culture flask surfaces using 0.25% trypsin/EDTA, re-suspended in DMEM and centrifuged at 1000 rpm for 6 minutes to remove the trypsin. Finally, the cells were diluted in DMEM to a concentration of 0.5 million cells per mL for the experiments.

Measurements of mRNA capture kinetics in microfluidic devices

To establish a benchmark, the pure synthetic fluorescently-labeled poly(A)$_{150}$-phi29 mRNA at 50 pM in a lysis/binding buffer (500 mM LiCl, 100 mM Tris-HCl, pH 7.5, 10 mM EDTA, 5 mM DTT, 1% lithium dodecyl sulfate) was used to determine the capture kinetics. Measurements were also performed with 50 pM mRNA in the presence of 250 pM and 1 nM of Alexa647-lableled poly(dT)$_{25}$ which can hybridize to the poly(A) tail on the mRNA to investigate the effect of the labeled poly(dT)$_{25}$ on the overall capture kinetics. To simplify the measurements, we used a device with straight channels of 2 mm width and 100 μm height fabricated on coverslips functionalized with poly(dT)$_{50}$ oligos. The mRNA solution was pulled into the microfluidic channel at a flow rate of 160 mm/s using a syringe pump and immediately time-lapse fluorescence images were acquired in both fluorescein and Alexa647 channels at the same field of view using a TIRF setup. Excitation was provided by a 488 nm laser for the fluorescein channel and a 642 nm laser for the Alex647 channel. The images were captured using 200 ms exposure and an EM gain of 20.

To simulate the condition used in our single-cell microfluidic device, we used simpler devices with 15 mm x 250 μm x 25 μm straight PDMS channels, which were fabricated and functionalized similarly, to measure the kinetics of mRNA capture from HeLa cell lysate. To prepare the lysate, the cultured cells were counted and mixed into lysis/binding buffer solution containing 2.5 nM of Cy3-poly(dT)$_{25}$ probe at a concentration of 1 cell per 3 nL, which is the volume of the processing chamber in our single-cell microfluidic device. Capture kinetics measurements were performed in a similar manner using a 532 nm laser for excitation. To quantify the non-

specific binding of the mRNA and the Cy3-labeled oligo probe to the surface, two control experiments were also performed, one with a channel that was not functionalized with poly(dT)$_{50}$ oligos, and one with a functionalized channel but only lysis/binding buffer and Cy3-poly(dT)$_{25}$ probe. The time-lapse images were analyzed and the single-molecule counts from the time-lapse images were plotted as a function of time.

Computational modeling of mRNA capture kinetics

mRNA capture is modeled as a one-dimensional diffusion-hybridization process. The mean squared displacement ($<x^2>$) of an mRNA molecule due to Brownian diffusion is calculated using the Einstein equation ($<x^2>=2Dt$) and the Stokes-Einstein equation ($D=k_BT/6\pi\eta R_h$), where D and R_h are the diffusivity and hydrodynamic radius of the mRNA molecule respectively. R_h can be approximated by $R_h=0.5(aLp/3)^{1/2}$, where a is the distance per base of single-stranded RNA ($a = 0.49$ nm), L is the contour length of the mRNA (number of bases) and p is the persistence length for single-stranded RNA ($p = 1.4$ nm).[35, 36] For simplicity, the hybridization of the poly(A) tail of the mRNA to the poly(dT)$_{50}$ oligos on the surface is treated as a pseudo first-order reaction since the poly(dT)$_{50}$ oligos are in large excess.

The entire process of mRNA capture by one dimensional diffusion and hybridization can be modeled using the diffusion equation:

$$\frac{\partial C}{\partial t} = D\frac{\partial^2 C}{\partial z^2} \qquad (1)$$

with the boundary conditions of a total reflector at the top surface ($\partial C(z=H,t)/\partial z=0$), a pseudo first-order irreversible hybridization reaction at the bottom surface ($\partial C(z=0,t)/\partial t=-kC(z=0,t)$) and an initial condition of uniform mRNA concentration ($C(z,t=0)=C_0$), where C is the concentration of the mRNA in the solution, k is the rate constant for the hybridization reaction which is independent of channel height, z is the perpendicular position above the surface of the channel and H is the height of the channel.

To investigate the capture kinetics of mRNA of various lengths in chambers with different heights, the partial differential equation (eq. 1) was solved numerically in MATLAB using the finite difference method. A mesh of 10^7 by 10^2 nodes was used to discretize the temporal by spatial components of the one dimensional diffusion model. To do so, first, the rate constant of the pseudo first-order hybridization reaction (k) was determined using the experimental kinetics data of poly(A)$_{150}$-phi29 mRNA capture in a 100 μm high channel. By inputting the calculated RNA diffusivity and channel height, the value of k was optimized so that the overall kinetics determined numerically by solving equation (1) using the finite difference method matches the overall experimentally measured kinetics data. The diffusivity of the RNA molecule is calculated using the Stokes-Einstein equation. Once k is determined, the theoretical kinetics data can be numerically computed for any channel height and RNA length. This model was also used to determine the hybridization reaction kinetics of mRNA capture from HeLa cell lysate in the presence of 2.5 nM Cy3-poly(dT)$_{25}$, as well as the synthetic mRNA in the presence of various concentrations of poly(dT)$_{25}$.

Capture of polyadenylated mRNA from single cells

Single HeLa cells were captured, isolated, and lysed in parallel using devices with 16 modules. Valve operations and fluid delivery were performed as described in our recent work.[32, 33] Several steps were performed to prepare the devices prior to the cell capture experiments. First, to reduce non-specific binding of cells, valve lines 2 and 3 were closed and the cell capture channels were passivated with a protein-free blocking buffer (PBS-T20, Thermo Fisher) by injecting the solution into the channels and incubating for >10 minutes. Second, the bottom reagent channels were filled with lysis/binding buffer solution containing 1 nM Alex647-poly(dT)$_{25}$ and 1 unit/μL of murine RNase inhibitor. Finally, the processing chambers were dried by a continuous flow of air through the channels.

Once a device was ready and mounted onto a microscope stage via an adaptor and valve lines 2 and 3 were actuated, a HeLa cell suspension was injected through the main channel at 1-10 μL per hour using an infusion syringe pump. The cells were captured one per trap automatically by hydrodynamic trapping as they flowed through the channel. The process was monitored by brightfield contrast microscopy. Then the inter-compartment valves (valves V1 and V2 in Fig. 1b) were closed to isolate the modules.

To process the cells, the individual cell in each module was pushed out of the trap and into the processing and mRNA capture chamber by opening valve line 2 and injecting the lysis/binding solution from the bottom reagent channel. After the air in the chamber was completely displaced (PDMS is permeable to air), valve line 2 was actuated to close the chamber. As the cell undergoes lysis in each compartment, the polyadenylated mRNA molecules are released into the chamber, diffuse and hybridize to the poly(dT)$_{50}$ oligos functionalized on the glass surface, while simultaneously hybridizing to the Alexa647-poly(dT)$_{25}$ in solution for detection. Bright-field microscopy was used to monitor the cell trapping and lysis process using a 10x objective. After at least ten minutes of incubation of mRNA in the capture chambers, the entire surface of each mRNA capture chamber was scanned and imaged with a 10 percent overlap between fields of view.

Single-molecule fluorescence imaging and image processing

Fluorescence imaging was performed using total internal reflection microscopy (TIRF) with an objective-based TIRF system. The system consists of a fully automated inverted fluorescence microscope equipped with an autofocus mechanism and a TIRF slider (AxioObserver Z1 and TIRF 3 Slider, Carl Zeiss) coupled to 4 lasers via a broadband optical fiber. A 100X oil/NA 1.46 objective lens was used for both laser excitation and fluorescent detection. A back-illuminated EMCCD camera (iXon3 897, Andor Technology) was used for imaging. Detail is provided in the text and Fig. S1 in ESI.

All image processing was performed with MATLAB (MathWorks). For each chamber, a montage was constructed by positioning each image tile in its proper location. Overlapping sections were merged by performing a maximum projection calculation to select which pixel value to incorporate. The background was removed by subtracting from the image using the morphological opening algorithm, calculated using a ball structured element with a radius of eight. The images were then thresholded to select pixels with a value above 50. To remove noisy pixels, a filter was applied to calculate the average density of thresholded spots around each pixel and a second round of thresholding was applied such that only selected pixels with at least two adjacently selected pixels were chosen. A labeling function was then employed to identify and index the separate objects in the binary image. At this point, spots with a small number of pixels were defined as a single molecule and the remaining objects were analyzed using the watershed transform to segment closely grouped molecules based on the topography in the original image.

A histogram of intensity values from all spots was utilized to select a mean intensity for a single mRNA transcript. An adjusted count for the number of transcripts present was estimated by dividing all intensity values by the approximated mean intensity of a single mRNA molecule.

Results

Device design, fabrication and operation

Our device is designed to integrate both single-cell capture and downstream processing in individual modules connected in serial for parallel processing of multiple cells. The cell traps of the modules are arranged in series while the processing chambers are arranged in parallel and can be isolated from one another by valves to enable parallel downstream processing. As illustrated in Figure 1, the dimensions of two paths in each trap chamber are designed such that the bulk of the incoming fluid is directed into the cell trap path. The traps can be tailored to capture cells of specific shape, size and elasticity.

Fig. 3 shows a photograph of a fabricated device (Fig. 3a), a contrast brightfield image of one module (Fig. 3b), and the results from computational modeling of fluid flow through a pair of hydrodynamic traps, one with a trapped cell and one empty (Fig. 3c). A closer examination shows that incoming fluid streamlines are directed into the cell trap path if the trap is empty. Once a single cell is captured and the trap is filled, the fluid streamlines are redirected to the bypass. Based on computational simulations and cell-capture experiments, we found that very high single-cell capture high efficiency can be achieved, with greater than 98% efficiency depending on the cell types and sizes. Example single-cell trapping movies (movies M1 and M2) are available in ESI.

Chemical bonding and selective functionalization of surfaces

Central to our design is the surface chemistry for efficient capture and analysis of single RNA molecules. This requires surfaces that have low non-specific binding to biomolecules and reagents such as fluorescently-labeled oligos to minimize sample loss and to reduce background noises for reliable single-molecule fluorescence imaging. For this purpose, we developed a method for chemical bonding and differential functionalization of the PDMS and glass surfaces.
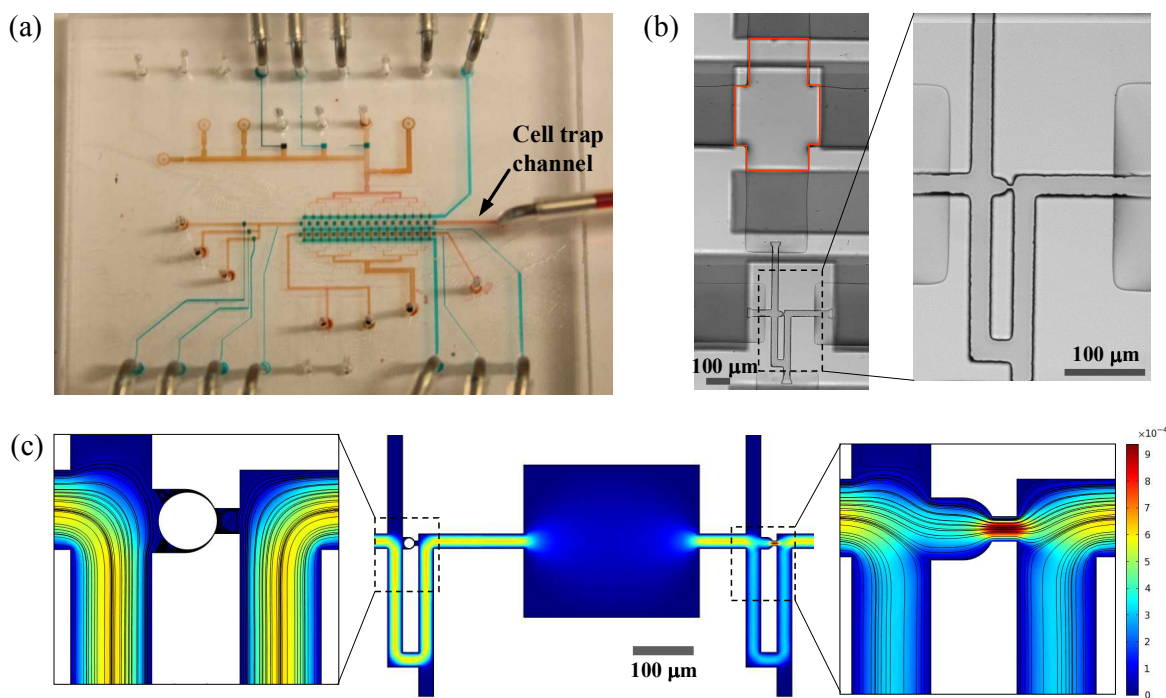
Lab on a Chip Accepted Manuscript

Fig. 3 Microfluidic device for capturing and counting of mRNA molecules from single cells. (a) A photograph of a functional device. The valve control lines are filled with a blue solution while the fluidic channels are filled with an orange solution. (b) A contrast brightfield image of an area containing a single module. The area outlined in red is the processing chamber where the cell is lysed and the released polyadenylated mRNA molecules are captured by hybridization to the poly(dT)$_{50}$ oligonucleotides covalently functionalized on the glass surface. (c) Modeling of fluidic flow through two traps in serial using finite element analysis. The zoom-in views show the fluidic flow streamlines through the two traps, one with a single cell (left) and one without any cell (right).
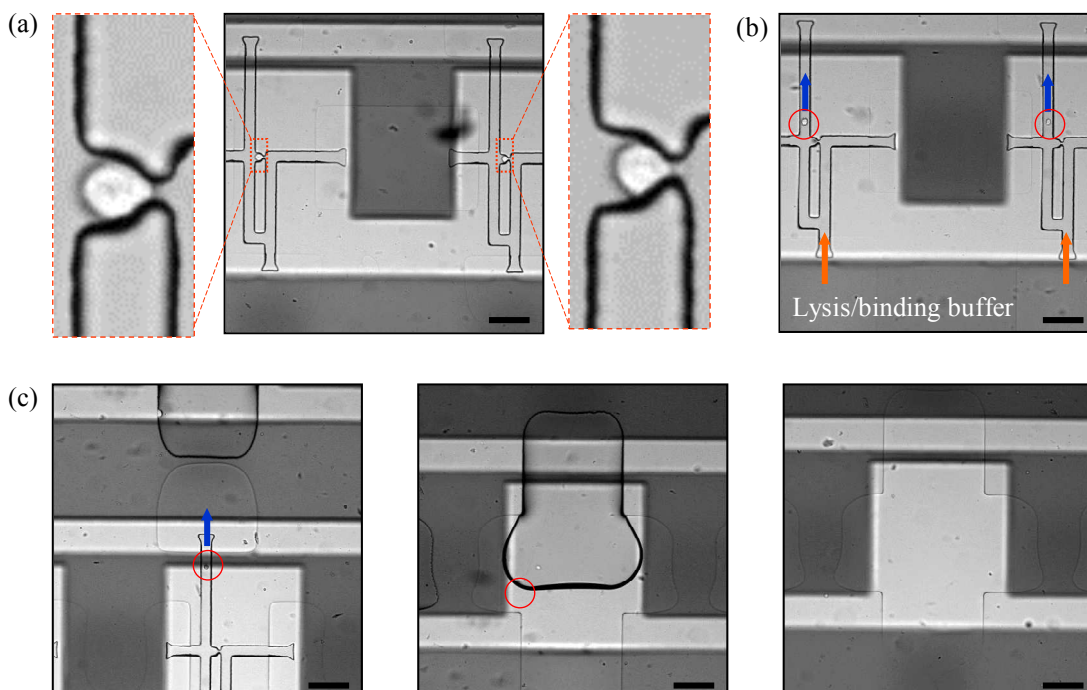

Fig. 4 Hydrodynamic capture and chemical lysis of single cells. (a) Bright-field micrograph of a portion of the device showing two modules, each with a single cell captured. The zoom-in views show that one cell (left) is larger than the other (right). (b) Following cell capture, the inter-module valves were closed and a lysis buffer was injected from the bottom reagent channel (orange arrows) to move the cells (in red circles) out of the trap site towards the processing chamber (blue arrows). (c) The further injection of the lysis buffer pushed the cell further toward (left panel) and into the processing chamber (middle panel) while the air was displaced from the chamber. Eventually the air was completely displaced and chamber was filled. The cell was fully lysed in the chamber and no longer observable (right panel). The scale bar is 100 μm.

As illustrated in Fig. 2, prior to the assembly of the glass-PDMS device, we functionalized the PDMS surface with epoxy groups and the glass surface with primary amine groups. This enables the chemical bonding of the PDMS to the glass coverslip without using plasma treatment which usually damages the functional groups on the surface. Moreover, our strategy enables the selective passivation of the PDMS surface inside the microfluidic channels with PEG which is known to prevent non-specific binding and fouling, and the selective covalent functionalization of only the glass surface with poly(dT)$_{50}$ oligos via a PEG linker. The selective functionalization enables the specific capture of polyadenylated RNA by hybridization onto the glass surface for processing and single-molecule imaging while the non-specific binding of RNA and other reagents to the PDMS surface is minimized.

Capture, isolation, and lysis of single cells

Fig. 4 shows the hydrodynamic capture and chemical lysis of single cells in a device. An image of two modules, each with a single cell trapped is shown in Fig. 4a. Following cell capture, the valves between the modules were closed to isolate each trapped cell from its neighbors. The valve between the cell trap and processing chamber which has been pre-filled with air is opened and the lysis/binding buffer was injected from the bottom reagent channel. Since the path from the backside of the cell trap has a lower fluidic resistance, the cell was dislodged from the trap site and pushed towards the processing chamber (Fig. 4b). As more lysis/binding solution was injected, the cell in the solution was pushed into the processing chamber by completely displacing the air in the chamber. An equal volume (~1.5 nL) of lysis buffer is mixed with the solution in the cell trap. The cell was lysed by the high concentration of the anionic detergent, lithium dodecyl sulfate (Fig. 4c). Cell lysis was observed to occur within seconds upon mixing with the lysis solution.

Kinetics of mRNA capture in a microfluidic device

The capture kinetics of the pure synthetic 1700-base fluorescein-labeled poly(A)$_{150}$-phi29 mRNA in a 100 μm high microfluidic channel in the absence of and presence of Alexa647-poly(dT)$_{25}$ at different ratios can be fit well with the diffusion-reaction model by optimizing the rate constant of the hybridization reaction. The kinetics data and fits are shown in Fig. 5. Table 1 lists the extracted time constants of the hybridization reaction, the time to reach 95% of total capture, the count of the captured mRNA and capture yields. In the absence of Alexa647-poly(dT)$_{25}$ oligos, the hybridization reaction on the surface is very rapid with a time constant of 6.1 s. As can be observed, the presence of the 25-base Alex647-poly(dT)$_{25}$,

which can hybridize to the 150-base poly(A) tail of the mRNA, affects the hybridization kinetics and capture yield. Since a maximum of 6 poly(dT)$_{25}$ oligos can hybridize to the 150-base poly(A) tail on each mRNA molecule, the ratio of poly(dT)$_{25}$ to mRNA is calculated as molar concentration ratio divided by a factor of 6. As the poly(dT)$_{25}$ to mRNA ratio increases from 0:1 to 0.83:1, and 3.3:1, the hybridization reaction time constant increases from 6.1 s to 7.5 s, and 68.3 s, respectively. The theoretical maximum number of molecules in a 50 pM mRNA solution over each field of view was obtained (~19,300) and used to calculate the capture yields. Considering that the mRNA molecules could be lost due to potential non-specific binding to the channels during sample transport, the yields are very likely lower than those of our single-cell devices, and reflect a lower limit for surface capture by hybridization and molecule counting.
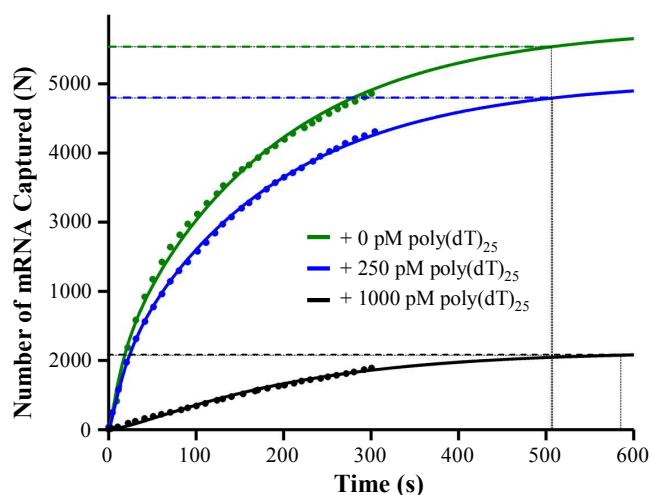

Fig. 5 Capture kinetics of synthetic polyadenylated fluorescently-labeled mRNA (poly(A)$_{150}$-phi29mRNA) in 100 μm high microfluidic channels. Shown are the kinetics data of capturing 50 pM mRNA in the presence of 0 pM, 250 pM and 1 nM of Cy3-poly(dT)$_{25}$ oligos. The data are fit to a reaction-diffusion model by optimizing the rate constant of the hybridization reaction on the surface. The dotted curves are the data and the solid lines are the model fits. The time constants of the hybridization reaction in the presence of 0, 250, and 1000 pM of Cy3-poly(T)$_{25}$ are determined to be 6.1 s, 7.5 s and 68.3 s, respectively. The horizontal dashed lines represent 95% completion of mRNA capture as approximated by the extrapolated fit. The vertical dashed lines correspond to the time at which 95% mRNA capture has occurred.

Table 1 Extracted parameters from the fits of capture kinetics data to the diffusion-hybridization model. The capture kinetics data were acquired using 50 pM of poly(A)150-phi29mRNA in the presence of various concentrations of Alexa647-poly(dT)$_{25}$ probe. The capture yield is calculated as percentage of the count of captured mRNA relative to the theoretical total number of mRNA in the solution above the measurement area.

Concentration of poly(dT)$_{25}$ (pM)	Hybridization time constant (s)	Time for 95% capture (s)	Captured mRNA count	Capture yield	R^2 of fit
0	6.1	506	5535	29%	0.997
250	7.5	507	4795	25%	0.999
1000	68.3	585	1077	5.6%	0.995

At a ratio of 0.83:1 which is below the level of the saturation of the poly(A) tails, the hybridization kinetics decreases only slightly. However, once the ratio is above saturation level (3.3:1 in this case), the capture kinetics decreases significantly. Intuitively, this is expected because the rate constant of the hybridization reaction between the poly(A) tail on the mRNA and the poly(dT)$_{50}$ on the surface is approximately linearly proportional to the squared root of the number of the available adenosine bases of the poly(A) tail,[37] and the fraction of available regions in the poly(A) tail for hybridization decreases drastically as the ratio is above saturation level. The capture yield or count is decreased as the ratio of poly(dT)$_{25}$ to the polyadenylated mRNA is increased. This indicates that the poly(A) tails of some mRNA molecules become saturated and inaccessible to capture by the poly(dT)$_{50}$ oligos on the surface. Interestingly, a significant fraction of the total mRNA is captured even though the labeled poly(dT)$_{25}$ is above saturation level.

Capture kinetics of mRNA from HeLa cell lysate

To simulate the single-cell mRNA capture kinetics experiments in the microfluidic device, our strategy is to add a fluorescently-labeled poly(dT)$_{25}$ oligo into the cell lysate to enable the real-time monitoring of the process by single-molecule fluorescence imaging using TIRF microscopy. Since the concentration of the total number of mRNA from a single HeLa cell is not known, we estimated the possible range and the concentration of the labeled poly(dT)$_{25}$ to be used for our measurements.
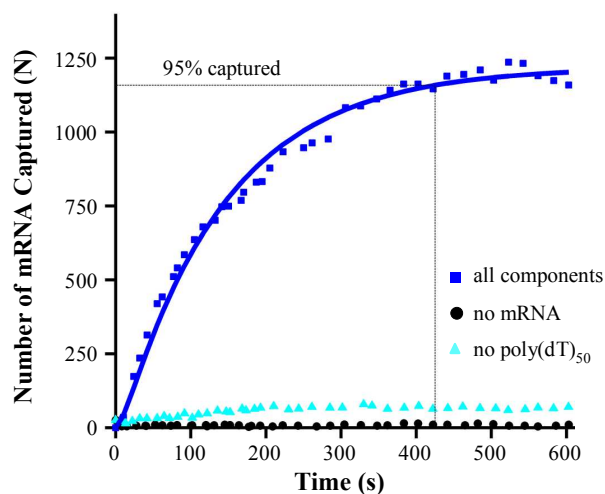

Fig. 6 Capture kinetics of polyadenylated mRNA from HeLa cell lysate in 25 μm high PDMS microfluidic channels. The concentration of the cell lysate is about 1 cell per 3 nL of lysis/binding buffer. Cy3-poly(dT)$_{25}$ probe was added to the cell lysate to a concentration of 2.5 μM to enable real-time monitoring of the capture kinetics. The kinetics data (blue squares) along with two control experiments (black dots and cyan triangles) are shown. In one control, cell lysate was not included (black dots, no mRNA), while in another control the surface of the device was not functionalized with poly(dT)$_{50}$ oligos. The curve of the mRNA capture data was fit to the diffusion-hybridization model (solid blue line). The time constant (1/k) of the hybridization reaction is determined to be 139 s. The time required to capture 95% of total mRNA (horizontal dotted gray line) is about 7 minutes (425 s).

We found that the addition of 2.5 nM of Cy3-poly(dT)$_{25}$ oligos to the HeLa cell lysate at a concentration equivalent to one cell in the volume of the processing chamber in our single-cell microfluidic device (~1 cell in 3 nL) allows for the simultaneous rapid capture and detection of the mRNA molecules.

The results from the kinetics experiments using HeLa cell lysate and a microfluidic device with 250 μm wide and 25 μm high straight channels are shown in Fig. 6. The kinetics data of mRNA capture from the HeLa cell lysate can be fit to our diffusion-hybridization model very well (R^2 = 0.988) using a 25 μm channel height and the parameters of a 1400-base RNA, which is the reported median length of the mRNA molecules in HeLa cells.[38] The time constant of the hybridization reaction was determined to be 139 s. The curve of the capture kinetics plateaus quickly around 500 s, and it takes only ~ 7 minutes to capture 95% of the total molecules that can be captured due to the use of the much lower 25 μm channel. In the absence of the Cy3-poly(dT)$_{25}$, the capture rate would have been much faster. Finally, in the chambers of the control experiments, there is only a constant and very low level of non-specific binding of the labeled probe oligos and mRNA throughout the course of the experiments. This confirms that our surface chemistry has very low non-specific binding and is suitable for single-molecule fluorescence imaging.

Computational modeling of mRNA capture kinetics

As can be observed in Fig. 5 and 6, the experimental mRNA capture kinetics data can be modeled very well using a one-dimensional diffusion equation with the boundary conditions of a total reflector at the top surface and a pseudo first-order hybridization reaction at the bottom surface. Fig. 7 shows the numerically simulated capture kinetics of RNA of four different lengths from 500 to 50,000 bases and two chamber heights of 25 μm and 100 μm using a time constant (1/k) of 6.1 s for the hybridization reaction that is determined from the experiment with the pure 1700-base poly(A)$_{150}$-phi29mRNA as described earlier. The extracted parameters and the times required for the RNA molecules diffuse across 25 μm and 100 μm high chambers calculated using the Einstein equation are listed in Table 2.

Table 2 Numerically simulated mRNA capture kinetics.

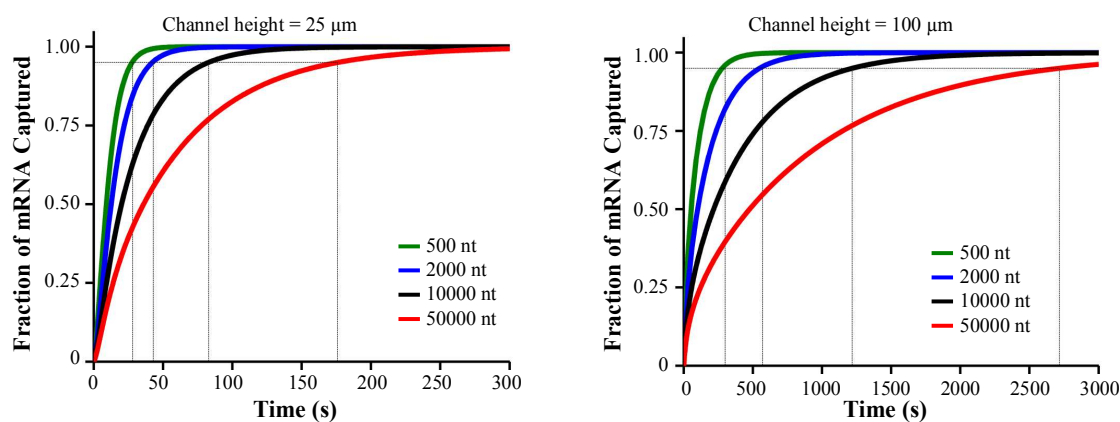| Channel Height	RNA Length (nt)	Time to 95% Capture (s)	Diffusion time (s)
25 μm	500	28	7.6
	2000	43	15
	10000	83	34
	50000	176	76
100 μm	500	278	122
	2000	549	245
	10000	1218	548
	50000	2718	1225

Fig. 7 Modeling and numerical simulations of mRNA capture kinetics. The kinetics were determined by numerically solving the diffusion equation (equation 1) using finite difference method and a time constant ($1/k$) of 6.1 s for the hybridization reaction. Shown are the capture kinetics of mRNA with lengths of 500 to 50000 bases in 25 μm (left panel) and 100 μm (right panel) high microfluidic chambers. The horizontal dotted gray line corresponds to 95% completion of total mRNA capture. The effect of mRNA length and channel height on the capture rate is distinctly visible and exaggerated for longer transcripts. In 25 μm chambers, mRNA capture is very rapid. Even for a 50000 base long mRNA, 95% capture can be achieved in 3 minutes (176 s).

With the exception of the very short RNA in 25 μm high chamber, the rate of mRNA capture is limited to a higher degree by diffusion. An increase in the length of mRNA and the height of the chamber results in slower capture rate. At 100 μm chamber height, the rate of mRNA capture is significantly reduced, especially for larger transcripts. Overall, the key finding is that mRNA with length up to 50000 bases can be captured to completion within 3 minutes in a chamber with 25 μm height.

Capture and enumeration of mRNA from single mammalian cells

Two microfluidic devices with 16 modules were fabricated and used for the single-cell mRNA capture experiments. A total of 9 cells were analyzed in 9 modules and 8 modules without any cell captured were used as control. In these experiments, 1 nM of Alexa647-poly(dT)$_{25}$ oligos was added into the lysis/binding buffer to label the polyadenylated mRNA for single-molecule imaging and counting.

The images were processed to count the total number of mRNA molecules from the individual cells. Fig. 8 shows an example fluorescence image and the objects recognized by our single-molecule selection algorithms overlaid on the image. As observed in Figure 8b, our algorithm can segment many adjacent spots into individual molecules or objects with high accuracy and the fluorescent intensities of the spots vary. The variation could be due to several factors. These include the variation in the number of
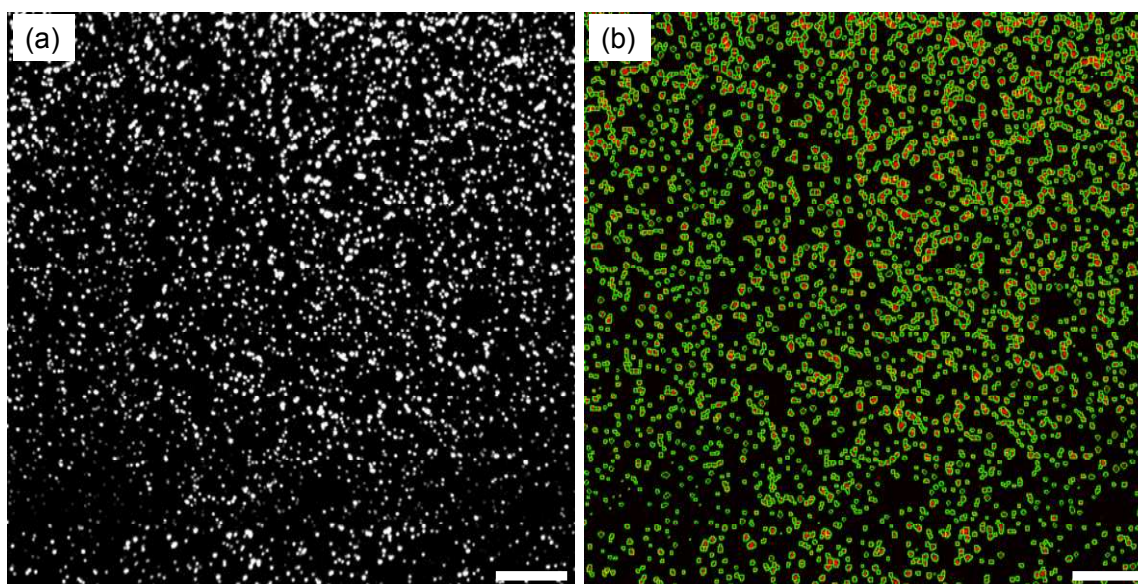

Fig. 8 Single-molecule fluorescence imaging and counting of captured mRNA from single cells. (a) A region from a montage image of an entire surface area of a chamber is shown. The background has been subtracted from the image. The region is close to where cell lysis occurred. (b) The same region that has been segmented with the single-molecule selection algorithm. Fluorescence intensity is shown in red and outlines of the molecules are shown in green. Scale bar: 10 μm.

Alexa647-poly(dT)$_{25}$ probe oligos that hybridize to each mRNA molecule due to the intrinsic variation in the length of the poly(A) tails of the different mRNA molecules, signal fluctuation inherent in single-molecule imaging, and possible co-localization of more than one molecule in the diffraction-limited spots (~320 nm resolution). Therefore, the raw counts represent the lower bound of the total poly(A) mRNA molecules in the single cells. To get a better estimate of the counts, an average intensity value of a single mRNA molecule is determined from the single-molecule cluster in a histogram with both the spots initially identified as isolated single molecules and the spots segmented with the watershed function (See Figure S2 in ESI).

An adjusted count is determined by dividing the total intensity by the average intensity value of a molecule.

The statistics of the counts are listed in Table 3. The count varies from 30,000 to 155,000 for the adjusted counts. The average mRNA count for all 9 channels containing single-cells is 69,752 with a coefficient of variation (CV) of 66%. In contrast, the adjusted counts of objects for the 8 control modules without any cell, which are primarily due to the non-specific binding of the Alexa647-poly(dT)$_{25}$ probe to the surface and auto-fluorescing impurities on the surface, are consistently low with an average of ~2500, less than 5% of the average count in the modules with single cells.

Table 3 Enumeration of mRNA molecules in single cells. Listed are the counts of the total number of polyadenylated mRNA molecules from 9 single cells measured with two separate devices. Listed are both the unadjusted raw counts of discrete objects identified on the image using a segmentation algorithm and the adjusted counts in which the potential number of molecules co-localized on each individual object has been accounted for by estimating the number of molecules based on intensity measurements.

		Device 1			Device 2					
		Cell 1	Cell 2	Cell 3	Cell 4	Cell 5	Cell 6	Cell 7	Cell 8	Cell 9
mRNA count	Adjusted (Raw)	40,080 (7,653)	30,406 (13,195)	56,771 (21,979)	136,709 (44,925)	40,192 (16,825)	154,734 (50,400)	37,100 (15,817)	87,256 (34,561)	44,521 (18,344)

Discussion

At present, no technology is available for direct single-molecule detection and enumeration of all mRNA transcripts from single cells. The microfluidic platform and methods described in this work represent a first attempt towards such a technology. Our strategy is to integrate single-cell capture and downstream processing into individual microfluidic modules connected in serial for scalable parallel analysis of multiple cells, and to selectively functionalize the glass surface in the processing chamber to enable the direct capture by hybridization and single-molecule imaging of polyadenylated mRNA molecules. We have shown experimentally that single cells can be captured with high efficiency using hydrodynamic traps which are tailored to capture cells of specific size and shape based on computational modeling. Critical to our design is the method we have developed for the differential passivation of the PDMS surface with PEG and the functionalization of the glass surface with poly(dT)$_{50}$ via a PEG linker to reduce non-specific binding to both surfaces and to enable the specific capture of polyadenylated mRNA molecules onto the glass for single-molecule fluorescence imaging and counting. The consistent low background from our control experiments with labeled probe but without cells underscores the suitability of our surface chemistry for single-molecule work.

Kinetics measurements of a pure 1700-base mRNA with a 150-base poly(A) tail in a 100 μm high microfluidic channel by real-time single-molecule imaging using TIRF microscopy showed that the mRNA capture fits to a one-dimensional diffusion-hybridization model. The time constant of the hybridization reaction on the surface was determined to be 6.1 s. mRNA capture reaches almost completion within 10 minutes. The presence of fluorescently-labeled poly(dT)$_{25}$ oligo affects the capture kinetics in an interesting manner. A concentration of poly(T)$_{25}$ below a level that saturates the poly(A) tails of the mRNA molecules (83% saturation in our experiments) decreases the capture kinetics only slightly, but a concentration above saturation level decreases the capture kinetics significantly. Additionally, an increase in the concentration of labeled poly(dT)$_{25}$ oligo reduces the yield of the capture, but does not completely block mRNA capture even when a concentration above saturation is used. We postulate that this likely could be due to the random nature of the hybridization of the poly(dT)$_{25}$ oligos along the longer poly(A) tails, leaving behind some short gapped regions of poly(A) that can still promote hybridization to the longer poly(dT)$_{50}$ oligos in the surface.

For simulated single-cell mRNA capture kinetics measurements in a chamber with the same dimensions of the microfluidic device for single-cell mRNA analysis, our strategy is to add a fluorescently-labeled poly(dT)$_{25}$ oligo into the cell lysate to hybridize to the poly(A) tails of the mRNA molecules so that the capture kinetics can be monitored in real time. We were able to determine a concentration of fluorescently-labeled poly(dT)$_{25}$ that enables the successful measurement of capture kinetics of polyadenylated mRNA from cell lysate equivalent to a single HeLa cell. In the presence of 2.5 nM of Cy3-poly(dT)$_{25}$, the mRNA capture kinetics is found to reach 95% completion by 425 s with a hybridization kinetics time constant of 139 s. This indicates that polyadenylated mRNA molecules released from a single cell can be completely captured within minutes by diffusion and hybridization. Because the hybridization kinetics is found to be slower than that of poly(A)$_{150}$-phi29 mRNA in the presence of saturation level of 1 nM poly(dT)$_{25}$ oligos (1:3.3), the poly(A) tails of the mRNA from the cells are presumably saturated to a higher degree. If the kinetics of the hybridization reaction follows a similar trend observed in the poly(A)$_{150}$-phi29 mRNA capture experiments, the capture yield would be less than 20%, potentially resulting in a total mRNA count 5 times or more lower than the expected true mRNA count in the absence of the labeled poly(dT)$_{25}$ oligos.

Our computational modeling of mRNA capture provides some useful insights into the mechanism of mRNA capture and how the length of the mRNA and the height of the microfluidic channel affect the capture kinetics. The rate constant of the hybridization reaction, which is dependent on the length of poly(A) tail but mostly independent of the length of the mRNA molecule, can be determined from experimental kinetics data using pure synthetic polyadenylated mRNA, poly(A)$_{150}$-phi29 mRNA. The rate of hybridization reaction is very fast with a time constant of about 6 s. If the chamber height is 25 μm, the capture kinetics is rate-limited to higher degree by the hybridization reaction for shorter transcripts (500 nt), but rate-limited to a higher degree by diffusion as the length of the mRNA increases. Overall the mRNA capture kinetics is very fast and is influenced modestly by the length of the mRNA molecules (see Fig. 6 and Table 2). Even for a 50000-base long mRNA, 95% capture can be achieved in 3 minutes. However, if the chamber height is increased to 100 μm, the capture kinetics is mostly rate-limited by diffusion and is slowed down significantly, especially for longer mRNA. These findings will be invaluable for the design of microfluidic devices and experiments for single-cell mRNA capture.

More importantly, we have, for the first time, demonstrated the ability to directly capture and count polyadenylated mRNA from single cells using a single microfluidic device. Total polyadenylated mRNA of 9 cultured HeLa cells were captured and counted. The adjusted counts vary from 30,000 to 155,000 molecules, with an average mRNA count of 69,752 and 66% CV. The large variation could be due to some intrinsic factors, including cell growth stages (we did not synchronize the cell growth) and stochastic nature of gene expression. In fact, the sizes of the individual cells are usually observed to be different. As shown in Figure 4A, the cell trapped at the left module is much larger than the one trapped at the right module. The variation could also be due to factors related to experimental measurements and image processing, for example, the variation of the number of labeled probes hybridized to transcripts with different poly(A) tail length, and limitation of the custom algorithms for single-molecule object recognition and counting.

Due to the use of labeled-poly(T)$_{25}$ oligo probe in the lysis/binding solution to allow for simultaneous capture and detection, the poly(A) tails of some mRNA molecules could potentially be saturated with poly(dT)$_{25}$ depending on the ratio of the labeled poly(dT)$_{25}$,probe to mRNA. This could significantly reduce the yield of capture of the mRNA by the poly(dT)$_{50}$ oligos onto the surface. We have observed this phenomenon in the experiments with synthetic poly(A)$_{150}$-phi29 mRNA in the presence of different ratios of poly(dT)$_{25}$ probe. The simulated single-cell mRNA capture kinetics experiment indicates that the capture yield could be below 20% of that of true complete capture in the absence of the poly(dT)$_{25}$ probe.

It has recently been reported that the median poly(A)-tail length for HeLa cells is 68 bases.[39] Because of such a relatively short median tail length, a large fraction of the total mRNA could potentially be either fully saturated with the poly(dT)$_{25}$, which would prevent the mRNA molecules from being captured onto the surface, or saturated by the poly(T)$_{50}$ oligos on the surface, which would prevent the hybridization of the labeled probe, resulting in uncounted mRNA molecules. In addition, some mRNA molecules may also bind non-specifically to the PDMS walls despite the passivation of the surface with PEG. All these factors could contribute to a significantly lower total mRNA count than the true count.

Given the uncertainties due to the limitations described above and the unavailability of a benchmark on absolute counting of total polyadenylated RNA molecules in single mammalian cells in the literature, further work will be required to improve and assess our technology in terms of absolute counting of mRNA of single cells. For example, single cells can be lysed in a lysis/binding buffer solution without a labeled poly(dT) probe oligo and the mRNA are captured onto the surface. The captured mRNA molecules can then be labeled by reverse transcription using fluorescently-labeled nucleotides and subsequently detected by single-molecule imaging. The total surface area of the processing chamber can be optimized and the captured mRNA can also be denatured and rehybridized to the poly(dT)$_{50}$ oligos to redistribute and thus even out the molecules on the surface to minimize the co-localization of the molecules for accurate counting. Our platform is also designed to be compatible with technologies for direct single-molecule nucleic acid detection either by hybridization using specific probes,[8-11, 40] or direct on-chip single-molecule sequencing.[16, 17, 41] Ultimately, we want to sequence the mRNA molecule or the reverse transcribed cDNA molecules by adapting and developing methods for single-molecule RNA sequencing or DNA sequencing. We are in the process of developing this capability in our laboratory.

Conclusions

Using a 1700-base synthetic fluorescently-labeled mRNA with 150-base poly(A) tail, we have demonstrated convincingly that the mRNA can be completely captured within minutes by diffusion and hybridization to poly(dT)$_{50}$ oligos selectively functionalized on glass the surface in a 25 μm high microfluidic chamber. Our modeling and numerical simulations of mRNA capture kinetics have also demonstrated that the hybridization reaction is very rapid with a time constant of ~6 s for mRNA with a 150-base poly(A) tail, and that short mRNA can be completely captured in less than one minute and even 50000-base long mRNA can be captured to almost completion within 3 minutes in a 25 μm high microfluidic chamber. By adding fluorescently-labeled poly(dT)$_{25}$ oligos into the HeLa cell lysate, we were able to simulate the capture kinetics of mRNA from single cells. Despite the reduced effective length or saturation of the poly(A) tails due to the hybridization of the poly(dT)$_{25}$ probe, the capture kinetics is still relatively rapid, with 95% capture in less than 7 minutes.

Using two separate integrated devices, we captured and enumerated polyadenylated mRNA molecules from 9 individual HeLa cells. The total counts of the polyadenylated mRNA from the individual cells are found to vary significantly from one cell to the other with a very large coefficient of variation. The total mRNA counts could be much lower than the true counts due to the use of the labeled poly(dT)$_{25}$ for detection and other factors. Further work will be required to improve and quantify capture efficiency and count accuracy, and potentially to enable identification of the mRNA by direct single-molecule sequencing.[16, 17, 41] Overall, our microfluidic devices and methods are designed to enable the entire workflow

from single cell isolation to mRNA capture and single-molecule imaging to be performed in a single device. The work described here has demonstrated these capabilities and has set the stage for the direct digital whole transcriptome profiling of single cells using a single integrated microfluidic device.

Acknowledgements

References

1. L. Cai, N. Friedman and X. S. Xie, *Nature*, 2006, **440**, 358-362.
2. D. G. Spiller, C. D. Wood, D. A. Rand and M. R. White, *Nature*, 2010, **465**, 736-745.
3. T. Kalisky and S. R. Quake, *Nature Methods*, 2011, **8**, 311-314.
4. S. C. Bendall and G. P. Nolan, *Nat Biotechnol*, 2012, **30**, 639-647.
5. A. Coulon, C. C. Chow, R. H. Singer and D. R. Larson, *Nat Rev Genet*, 2013, **14**, 572-584.
6. P. M. Lizardi, X. Huang, Z. Zhu, P. Bray-Ward, D. C. Thomas and D. C. Ward, *Nat Genet*, 1998, **19**, 225-232.
7. X. B. Zhong, P. M. Lizardi, X. H. Huang, P. L. Bray-Ward and D. C. Ward, *Proc Natl Acad Sci U S A*, 2001, **98**, 3940-3945.
8. Y. Zhou, M. Calciano, S. Hamann, J. H. Leamon, T. Strugnell, M. W. Christian and P. M. Lizardi, *Exp Mol Pathol*, 2001, **70**, 281-288.
9. J. M. Levsky, S. M. Shenoy, R. C. Pezo and R. H. Singer, *Science*, 2002, **297**, 836-840.
10. C. Larsson, I. Grundberg, O. Soderberg and M. Nilsson, *Nat Methods*, 2010, **7**, 395-397.
11. S. Hocine, P. Raymond, D. Zenklusen, J. A. Chao and R. H. Singer, *Nat Methods*, 2013, **10**, 119-121.
12. F. Tang, C. Barbacioru, Y. Wang, E. Nordman, C. Lee, N. Xu, X. Wang, J. Bodeau, B. B. Tuch, A. Siddiqui, K. Lao and M. A. Surani, *Nat Methods*, 2009, **6**, 377-382.
13. A. R. Wu, N. F. Neff, T. Kalisky, P. Dalerba, B. Treutlein, M. E. Rothenberg, F. M. Mburu, G. L. Mantalas, S. Sim, M. F. Clarke and S. R. Quake, *Nat Methods*, 2014, **11**, 41-46.
14. F. Tang, K. Lao and M. A. Surani, *Nat Methods*, 2011, **8**, S6-11.
15. Q. Deng, D. Ramskold, B. Reinius and R. Sandberg, *Science*, 2014, **343**, 193-196.
16. F. Ozsolak, A. R. Platt, D. R. Jones, J. G. Reifenberger, L. E. Sass, P. McInerney, J. F. Thompson, J. Bowers, M. Jarosz and P. M. Milos, *Nature*, 2009, **461**, 814-818.
17. F. Ozsolak and P. M. Milos, *Methods Mol Biol*, 2011, **733**, 51-61.
18. I. D. Vilfan, Y. C. Tsai, T. A. Clark, J. Wegener, Q. Dai, C. Yi, T. Pan, S. W. Turner and J. Korlach, *J Nanobiotechnology*, 2013, **11**, 8.
19. V. Bhargava, S. R. Head, P. Ordoukhanian, M. Mercola and S. Subramaniam, *Sci Rep*, 2014, **4**, 3678.
20. Y. Marcy, T. Ishoey, R. S. Lasken, T. B. Stockwell, B. P. Walenz, A. L. Halpern, K. Y. Beeson, S. M. Goldberg and S. R. Quake, *PLoS Genet*, 2007, **3**, 1702-1708.
21. S. Islam, A. Zeisel, S. Joost, G. La Manno, P. Zajac, M. Kasper, P. Lonnerberg and S. Linnarsson, *Nat Methods*, 2014, **11**, 163-166.
22. A. M. Streets, X. Zhang, C. Cao, Y. Pang, X. Wu, L. Xiong, L. Yang, Y. Fu, L. Zhao, F. Tang and Y. Huang, *Proc Natl Acad Sci U S A*, 2014, **111**, 7048-7053.
23. A. A. Powell, A. H. Talasaz, H. Zhang, M. A. Coram, A. Reddy, G. Deng, M. L. Telli, R. H. Advani, R. W. Carlson, J. A. Mollick, S. Sheth, A. W. Kurian, J. M. Ford, F. E. Stockdale, S. R. Quake, R. F. Pease, M. N. Mindrinos, G. Bhanot, S. H. Dairkee, R. W. Davis and S. S. Jeffrey, *PLoS One*, 2012, **7**, e33788.
24. V. Sanchez-Freire, A. D. Ebert, T. Kalisky, S. R. Quake and J. C. Wu, *Nat Protoc*, 2012, **7**, 829-838.
25. M. H. Dominguez, P. K. Chattopadhyay, S. Ma, L. Lamoreaux, A. McDavid, G. Finak, R. Gottardo, R. A. Koup and M. Roederer, *Journal of Immunological Methods*, 2013, **391**, 133-145.
26. A. K. White, M. VanInsberghe, O. I. Petriv, M. Hamidi, D. Sikorski, M. A. Marra, J. Piret, S. Aparicio and C. L. Hansen, *P Natl Acad Sci USA*, 2011, **108**, 13999-14004.
27. L. He, A. Kniss, A. San-Miguel, T. Rouse, M. L. Kemp and H. Lu, *Lab Chip*, 2015, **15**, 1497-1507.
28. Y. Yu, B. Li, C. A. Baker, X. Zhang and M. G. Roper, *Anal Chem*, 2012, **84**, 2825-2829.
29. J. Wen, X. Yang, K. Wang, W. Tan, L. Zhou, X. Zuo, H. Zhang and Y. Chen, *Biosens Bioelectron*, 2007, **22**, 2759-2762.
30. W. H. Tan and S. Takeuchi, *Proc Natl Acad Sci U S A*, 2007, **104**, 1146-1151.
31. M. A. Unger, H. P. Chou, T. Thorsen, A. Scherer and S. R. Quake, *Science*, 2000, **288**, 113-116.
32. H. S. Lee, W. K. Chu, K. Zhang and X. Huang, *Lab Chip*, 2013, **13**, 3389-3397.
33. A. P. Hsiao, K. D. Barbee and X. Huang, *Proc Soc Photo Opt Instrum Eng*, 2010, **7759**, pii: 77590W_77591, doi: 77510.71117/77512.861563.
34. B. H. C. Nae Yoon Lee, *Langmuir*, 2009, **25**, 7.
35. B. Tinland, A. Pluen, J. Sturm and G. Weill, *Macromolecules*, 1997, **30**, 5763-5765.
36. H. Chen, S. P. Meisburger, S. A. Pabit, J. L. Sutton, W. W. Webb and L. Pollack, *Proc Natl Acad Sci U S A*, 2012, **109**, 799-804.
37. J. G. Wetmur and N. Davidson, *J Mol Biol*, 1968, **31**, 349-370.
38. S. S. Sommer and J. E. Cohen, *J Mol Evol*, 1980, **15**, 37-57.
39. A. O. Subtelny, S. W. Eichhorn, G. R. Chen, H. Sive and D. P. Bartel, *Nature*, 2014, **508**, 66-71.
40. G. K. Geiss, R. E. Bumgarner, B. Birditt, T. Dahl, N. Dowidar, D. L. Dunaway, H. P. Fell, S. Ferree, R. D. George, T. Grogan, J. J. James, M. Maysuria, J. D. Mitton, P. Oliveri, J. L. Osborn, T. Peng, A. L. Ratcliffe, P. J. Webster, E. H. Davidson, L. Hood and K. Dimitrov, *Nat Biotechnol*, 2008, **26**, 317-325.
41. T. D. Harris, P. R. Buzby, H. Babcock, E. Beer, J. Bowers, I. Braslavsky, M. Causey, J. Colonell, J. Dimeo, J. W. Efcavitch, E. Giladi, J. Gill, J. Healy, M. Jarosz, D. Lapen, K. Moulton, S. R. Quake, K. Steinmann, E. Thayer, A. Tyurina, R. Ward, H. Weiss and Z. Xie, *Science*, 2008, **320**, 106-109.